Passivating effect of ternary alloyed AgZnSe shell layer on the structural and luminescent properties of CdS quantum dots

Adegoke, Oluwasesan; Montaseri, Hanieh; Nsibande, Sifiso A.; Forbes, Patricia B.C.

Published in:
Materials Science in Semiconductor Processing

DOI:
10.1016/j.mssp.2018.10.025

Publication date:
2019

Passivating effect of ternary alloyed AgZnSe shell layer on the structural and luminescent properties of CdS quantum dots

Oluwasesan Adegoke, Hanieh Montaseri, Sifiso A. Nsibande, Patricia B.C. Forbes *

Department of Chemistry, Faculty of Natural and Agricultural Sciences, University of Pretoria, Lynnwood Road, Pretoria 0002, South Africa

*Corresponding author: *Email address:* adegoke.sesan@mailbox.co.za (O. Adegoke), patricia.forbes@up.ac.za (P.B.C. Forbes)

Abstract

The surface passivation of luminescent CdS quantum dots (QDs) via epitaxial overgrowth of new alloyed ternary AgZnSe shell layer is reported here. Two synthetic fabrication strategies were used to tune the optical properties of CdS/AgZnSe core/alloyed shell QDs across the visible region. Transmission electron microscopy, powder X-ray diffraction, Raman, UV/vis and fluorescence spectrophotometric techniques were used to characterize the nanocrystals. Analysis of the internal structure of the QDs revealed that homogeneity of the particle reduced as the size increased, thus indicating that the QDs growth transitioned from an interfacial epitaxial homogenous state to a heterogeneous state. The crystal structure of the QDs revealed a distinct zinc-blende diffraction pattern for CdS while CdS/AgZnSe core/alloyed shell QDs kinetically favoured a phase change process from the zinc-blende phase to a wurtzite phase. Analysis of the photophysical properties revealed varying degrees of interfacial defect state suppression in CdS/AgZnSe QDs which was dependent on the QDs size. Specifically, the fluorescence quantum yield (QY) of CdS/AgZnSe QDs was at most ~5-fold higher than the CdS core and varied from 35-73%. We found that band gap modulation via the synthetic fabrication strategy employed, influenced the optical properties of the core/alloyed shell QDs. The CdS/AgZnSe QDs produced in this work hold great promise in light-emitting optoelectronic applications.

KEYWORD: Quantum dots; surface defects; photoluminescence; quantum yield; alloyed

1. Introduction

The wide electro-luminescent applications of colloidal semiconductor quantum dot (QD) nanocrystals in various fields of chemistry, biology and physics, stem from their unique optoelectronic properties **[1,2]**. Particularly, the size-dependent optical and electronic properties of QDs which are governed by the associated quantum confinement feature, allows tuning of the photoluminescence (PL) emission from the ultraviolet/visible (UV/vis) region to the far infra-red region **[3-6].** In contrast to bulk semiconductors in which the surface represents a tiny fraction of the bulk material, colloidal QDs have their size typically in the range of 2–10 nm. This unique characteristic enables a large number of atoms to be embedded on the QD surface **[7]**.

The QD surface represents a highly sensitive region that is exposed to its surrounding environment (matrices, solvents and various other species in solution) and it is typically coordinated by chemical ligands, surfactants or stabilizers that influence the QD optoelectronic properties **[7].** The synergistic effects of precursor material which create low numbers of coordinated surface atoms may lead to highly reactive or localized electronic sites that are susceptible to redox and chemical processes. Thus, it is very likely for midgap, shallow or deep surface defect states to be formed and induce the pathway for poor PL properties. The characteristic phenomenon is nonradiative recombination exciton (electron and hole) states associated with low PL quantum yield (QY) **[8,9]**. One of the widely used strategies to eliminate surface traps is to passivate the QD core surface with a wider band gap shell material **[10-13]**. This strategy shifts the surface defects to the outer domain of the shell layer, thus improving the PL QY **[4].** The electron and hole being localized in the core, represents a signature process associated with the low probability of the outer surface state being subjected to trapped photogenerated charge carriers **[14,15]**.

Over the past two decades, the most studied class of semiconductor QDs are the group II-VI metal chalcogenides with CdSe-based QDs being the most popular for fabricating new synthetic routes **[16]**, shell passivation **[17],** ligand dynamics **[18]** and alloying **[19].** On the other hand, CdS nanocrystals are probably the second most studied QD system **[20-23]**, exhibiting an exciton Bohr radius of 3.0 nm **[24]** and a bulk band gap of 2.48 eV **[25].** Its characteristic PL emission is known to be highly prone to surface defects which results in low PL QY **[26].** Nonetheless, it is widely used as a shell layer to overcoat the surface of CdSe-based QDs. The well-known strategy to isolate the exciton wave function from the surface of the core QDs with embedded surface defects and dangling bonds is to coat with a shell layer of a wide band gap **[27]**. However, it is important to note that lattice mismatch between the core and binary shell material at the interface can also induce surface defects that degrade the luminescence of the core/shell QDs, thus lowering the PL QY **[28]**.

Another strategy which has drawn significant interest in improving the PL QY of binary core QDs is to coat the surface with an alloyed ternary shell layer**.** Alloyed QDs (AB_xC_{1-x}) have become important in mainstream nanoscale optical engineering due to the added degree of freedom in tuning the exciton energy for either extended PL emission range or improved optical properties **[29-32].** The coating of an alloyed ternary shell around binary core QDs to improve the PL efficiency has mostly been reported for CdSe-based QDs **[33,34]** with rare reports for CdS-based QDs **[13].** It is noteworthy that apart from the formation of a smooth gradient band gap, the lattice strain of the core/shell QDs can be relaxed due to alloying **[35].** Furthermore, it has been demonstrated that shell alloying suppressed Auger exciton recombination in core/alloyed shell/ shell QDs, thus increasing the PL QY **[36].**

Overcoating a shell layer around the CdS core to improve the PL QY of QDs has rarely been studied. Thus, in this paper, we report on a new strategy to suppress the surface defect states of CdS QDs by coating with a new ternary alloyed shell layer. CdS QDs, characterized by low PL QY due to embedded surface defects were synthesized in this work via the organometallic synthetic route. We have demonstrated for the first time that improved PL QY in CdS QDs can be achieved via passivation with a ternary alloyed AgZnSe shell layer. To the best of our knowledge, our work is the first to overcoat a AgZnSe shell around CdS core QDs with the sole aim of suppressing interfacial defect states in the core QDs. The organic-phase CdS/AgZnSe core/alloyed shell QDs produced in this work hold great promise in light-emitting optoelectronic applications.

2. Experimental section

2.1. Materials

Cadmium oxide (CdO), myristic acid, trioctylphosphine oxide (TOPO), hexadecylamine (HDA), trioctylphosphine (TOP), octadecene (ODE), oleic acid, sulphur (S), L-cysteine, diethylzinc (Et_2Zn) and zinc oxide (ZnO) were purchased from Sigma Aldrich. Silver nitrate ($AgNO_3$) was purchased from Saarchem. Selenium (Se) was purchased from Merck. Methanol, acetone, hexane and chloroform were purchased from ACE Chemicals.

2.2. Characterization

UV/vis absorption spectra were obtained using a Cary Eclipse (Varian) spectrophotometer. PL emission measurements were carried out using a Horiba Jobin Yvon Fluoromax-4 spectrofluorometer. Powder X-ray diffraction (PXRD) measurements were determined using a Cu(Kα) radiation (λ=1.54184 Å) on a Bruker D2 Phaser. Transmission electron microscopy (TEM)

images were produced using a JEOL JEM 2100F operated at 200 kV. Raman spectra were recorded using a WITec Alpha 300 micro-Raman imaging system with a 488 nm excitation laser and CCD detector at ambient temperature with the laser power below 2 mW in order to reduce heating effects.

2.3. Preparation of the precursors

2.3.1. TOPSe

To prepare the Se precursor, 0.12 g Se was dissolved in 5 mL TOP and sonicated until complete dissolution of Se, thus resulting in a clear solution. The solution was then stirred at room temperature prior to use and was stable for 3 days.

2.3.2. TOPZn

To prepare the Zn precursor from Et_2Zn, 1.93 g TOPO was firstly dissolved in 10 mL ODE and 5 mL of oleic acid. The solution was then heated up until the complete dissolution of TOPO surfactant, thus resulting in a clear solution. Thereafter, 2 mL Et_2Zn and 1 mL TOP were added and the solution was stirred at room temperature before use.

To prepare the Zn precursor from ZnO, 0.4 g ZnO was added to a mixture of 15 mL ODE and 10 mL oleic acid and sonicated for a few minutes. Thereafter, the precursor solution was stirred at room temperature prior to use.

2.3.3. TOPAg

Ag precursor was prepared by mixing 0.5 g $AgNO_3$ with 5 mL TOP. The solution was then heated up until complete dissolution of the $AgNO_3$ which was evident by the change in colour from colourless to brownish black.

2.3.4. TOPS

To prepare the TOPS precursor used in method 1 synthesis of CdS/AgZnSe QDs (refer to section 2.4), 1.93 g TOPO was first dissolved in 15 mL ODE and 10 mL oleic acid followed by the addition of 0.16g S and 1 mL TOP. For method 2 synthesis of CdS/AgZnSe QDs (section 2.5), 1.93 g TOPO was dissolved in 10 mL ODE and 5 mL oleic acid, then 0.08 g S and 1 mL TOP was added thereafter. The solutions were sonicated and heated up to aid complete dissolution of the S and thereafter stirred at room temperature prior to use.

2.4. Synthesis of CdS/AgZnSe core/alloyed shell QDs (method 1)

The synthesis of CdS/AgZnSe core/alloyed shell QDs was carried out via the organometallic one-pot synthetic route but with modifications **[37].** Complexation between the Cd ion, surfactants and capping ligands was formed by mixing 1.3 g CdO, 1.2 g myristic acid, 1.93 g TOPO and 1.2 g HDA with 50 mL ODE and 30 mL of oleic acid. The solution was bubbled with Ar gas and heated up until complete dissolution of the Cd ion which was evident by a change in colour of the solution from pale brown to colourless. At ~220 °C, TOPS solution was added into the Cd precursor solution to form the CdS core QDs. Once satisfactory growth of the QD core was achieved, a fraction of the growth solution was injected into a beaker. To form the core/alloyed shell QDs, 1 ml of TOPSe solution was added into the CdS growth solution followed swiftly by the addition of 1 mL TOPAg and TOPZn (using ZnO). Portions of the core/shell QDs were taken out at different time intervals.

158 *2.5. Synthesis of CdS/AgZnSe QDs (method 2)*

159 Method 2 synthesis was carried out according to the fabrication steps detailed in method 1 but with
160 slight modifications of the precursor concentrations. For the complexation of Cd ion with the
161 precursor materials, 2 mL TOP, 0.4 g CdO, 0.6 g HDA and 0.6 g myristic acid were mixed with
162 20 mL ODE and 15 mL oleic acid. The synthetic process of method 1 was therefater followed by
163 adding TOPS (prepared specifically for method 2) to form the CdS QDs. Formation of the
164 core/alloyed shell QDs was followed according to method 1 except that TOPZn prepared from
165 ET_2Zn was used.

166

167 ## 3. Results and discussion

168 *3.1. Fabrication of the QDs*

169 One-pot organometallic synthesis of metal precursors in the presence of surfactants, organic-
170 capping ligands and a non-coordinating solvent (ODE) was used to engineer the structure of the
171 QDs. It is well known that the growth kinetics influences the PL emission and absorption evolution
172 of the QDs **[38]**. The nature of the precursor material with respect to the concentration, quantity,
173 time of injection, temperature and the interplay between them are reaction conditions that influence
174 the growth of the QDs. We have therefore exploited these reaction conditions to engineer the
175 optical properties of CdS/AgZnSe core/alloyed shell QDs.

176 In method 1 synthesis, higher quantities of the Cd metal precursor, surfactants, organic ligands and
177 the non-coordinating solvent were used to aid the Cd-precursor complexation for the subsequent
178 nucleation and growth of CdS QDs. Conversely, lower concentrations of the Cd precursor,
179 surfactants and ligands were employed in method 2 synthesis of the QDs. Before adding the TOPS
180 precursor, the Cd precursor solution was heated up to >200 °C to aid complete dissolution and

complexation of the Cd precursor. The change in colour of the solution from brown to colourless confirmed the complexation process which was accompanied by injection of the TOPS precursor. As the CdS core QDs nucleated, the temperature of the growth solution increased steadily and was accompanied by a concomitant change in the colour. During this period, a fraction of the CdS core QDs was removed in order to probe the structural and optical properties thereof in comparison to the core/alloyed shell QDs.

The temperature at which the AgZnSe alloyed shell was overcoated on the CdS core surface is very crucial to the overall optical properties of the CdS/AgZnSe core/alloyed shell QDs. At higher temperature and longer reaction time, CdS QDs size distribution is expected to deteriorate and lead to broadening of the spectral line widths. On the other hand, overcoating the shell layer at relatively low temperature could either reduce the crystallinity of CdS/AgZnSe core/alloyed shell QDs or lead to incomplete decomposition of the precursor materials **[39]**. Therefore, an appropriate temperature was determined independently for each method used to fabricate the core/alloyed shell QDs. The concentration and rate at which the AgZnSe shell precursor is added is also crucial in influencing the optical properties of the QDs. Slow addition of the precursor shell materials prevents homogenous nucleation and induces most of the AgZnSe shell to grow heterogeneously on the CdS nuclei. Hence, the precursor solutions for the shell layering were injected into the CdS growth solution in swift succession. Addition of TOPSe, TOPZn and TOPAg precursors to the CdS growth solution triggered a progressive change in the colour of the solution from orange to red and to dark brown. Different sizes of the CdS/AgZnSe QDs were thereafter harvested at different time intervals whilst the QDs were purified with acetone, chloroform/acetone and chloroform/acetone/ethanol mixture.

3.2. Structural properties

3.2.1. Surface morphology

TEM analysis was used to qualitatively probe the internal structure of the QDs with respect to the shape, size distribution, and shell coverage. Fig. 1A-C shows the TEM images of three different-sized CdS QDs with average sizes of 6.0±0.5, 6.5±0.5 and 7.5±1.2 nm respectively. Our aim was to synthesize uniform-sized CdS QDs in order to effectively understand the structural effects of shell layering. Looking closely at each TEM micrograph, a uniform size distribution, embedded with a mixture of spherical and quasi-spherical shapes was observed. Thus, the monodispersed particle size distribution provides direct indication of homogenous nucleation and growth of the core QDs.

Alloyed semiconductor QD nanocrystals can be grouped as having either a gradient internal structure derived from varying the alloy composition or a uniform internal structure ascribed to homogenous alloying. In our work, a fixed composition of the shell precursor was used to engineer the structure of the core/alloyed shell QDs. Fig. 2A-D shows the representative TEM images of CdS/AgZnSe core/alloyed shell QDs synthesized via method 1 with average particle sizes of 5.1±0.6, 5.5±0.7, 7.9±1.6 and 9.1±1.9 nm respectively. The striking feature was the decrease in the core/alloyed shell QDs particle size relative to the core which is an unusual phenomenon as the size of the core/shell QDs is expected to increase after shell passivation. Since shell passivation of the 7.5 nm CdS QDs led to rapid nucleation and growth of the different sized CdS/AgZnSe QDs, it is imperative to suggest that either CdS was buried within the shell domain or an intermediate formation of CdS/CdSe occurred before the growth of CdS/AgZnSe QDs.

As the CdS/AgZnSe QDs grew, a steady transformation in the particle morphology with respect to the size distribution was observed. The homogeneity of the particle reduced as the size

increased, thus indicating that the QDs growth transitioned from an interfacial epitaxial homogenous state to a heterogeneous state. During the period of harvesting each of the different-sized QDs, the temperature of the solution increased from ~240 – 310 °C and this should tentatively influence the nucleation and growth of the QDs. It is also noteworthy to emphasize that the transition in homogeneity of the QDs correlated significantly to the shape engineering of the particle. Looking closely at the TEM monograph of 7.9 nm and 9.1 nm-sized CdS/AgZnSe QDs (Fig. 2C and 2D), the emergence of trigonal-shaped particles was observed. Tentatively, we could attribute the shape engineering of the QDs to the passivating effect of AgZnSe shell, thus implying that the electronic structure of CdS/AgZnSe QDs led to different confinement levels for electron and hole. The hole may be strongly confined to the CdS core while the electron may be delocalised into the shell layer **[40].**

Three different sizes of CdS/AgZnSe QDs were harvested using method 2 synthetic route. The corresponding TEM images and particle size histograms are shown in Fig. 3. The particle size distribution revealed a prolate heterogeneous particle morphology, resembling an anisotropic-like growth pattern. The anisotropic growth pattern can be understood in terms of the reaction conditions used in the synthesis as it applies to low reactivity precursors and low volume of coordinating solvent. Under these reaction conditions, CdS/AgZnSe heteroepitaxial growth is kinetically controlled (i.e., AgZnSe formation at the surface is the rate-limiting step, rather than the precursor diffusion) and slow. Thus, the high reactivity of the Ag, Zn and Se of the AgZnSe shell layer will favour anisotropic-type growth **[41].**

Generally, the mechanism of nucleation and growth of CdS/AgZnSe QDs can be understood in terms of Ostwald ripening. At relatively low temperature (220–240 °C), Ostwald ripening dominated as a result of dissolution and surface energy of small particles which redissolve to allow

subsequent growth of larger particles. At higher temperature (>260 °C), Brownian motion will increase in the synthetic system due to higher thermal energy. Hence it is more likely that the increase in motion will allow the particles to interact at the exact crystallographic orientation, leading to orientated attachment **[42]**.

3.2.2. Crystal phase analysis

The crystal structure of CdS core and CdS/AgZnSe QDs was studied using PXRD. From the diffraction pattern of the CdS core (Fig 4), a pure zinc-blende crystal structure with three prominent peaks at planes {111}, {220} and {311} was observed. The three planes exhibited Bragg angles at 26.5°, 43.9° and 51.9° respectively. Comparison of the diffraction pattern of CdS/AgZnSe core/alloyed shell QDs with CdS QDs reveal notable differences. Firstly, the three-notable peaks (associated with zinc-blende crystal structure) present in CdS were observed in CdS/AgZnSe$_{588}$. However, the appearance of four additional peaks between 30–40° and two additional peaks at higher Bragg angle (47.6° and 56.8°) provides direct evidence that the shell alloying process induced crystal phase changes in the QDs. Since the CdS/AgZnSe QDs size was tuned by fixed shell alloying, it is interesting to note the phase transition changes in the core/alloyed shell QDs. As the size of CdS/AgZnSe QDs increased, a steady transformation in the diffraction pattern as it relates to changes in the diffraction peaks was observed. A close assessment of the diffraction pattern of CdS/AgZnSe$_{593}$, revealed detailed formation of a duplet peak at low Bragg angle which can be attributed to the steady phase transition from a zinc-blende diffraction pattern to a wurtzite diffraction pattern. Further growth of the core/alloyed shell QDs led to the formation of a triplet peak at low angle as observed from the diffraction pattern of CdS/AgZnSe$_{599}$. Further assessment of the diffraction pattern of CdS/AgZnSe$_{601}$ revealed the formation of a pure wurtzite diffraction

pattern. Thus, is can be concluded that CdS core QDs favoured a zinc-blende crystal structure while the CdS/AgZnSe core-alloyed QDs kinetically favoured a phase change from a zinc-blende diffraction pattern to a wurtzite diffraction pattern.

3.2.3. Raman analysis

Core/shell QDs have been proven to reduce Auger recombination rates, which is important in multiexciton recombination and OFF/ON blinking process **[43].** It is also believed that the core/shell interfacial alloying region is associated with a graded interface **[44].** Hence, the potential of Raman to probe the internal structure of the core/alloyed shell QDs interface was investigated. Fig. 5 shows the Raman spectra for CdS core and the different-sized CdS/AgZnSe QDs. The similarities with reference to the peak position of CdS longitudinal optical phonon (LO) bulk frequency at ~300 cm^{-1} and CdS overtone at ~600 cm^{-1} with those of $CdS/AgZnSe_{588}$ and $CdS/AgZnSe_{93}$, provides strong indication of the homogenous growth of the core/alloyed shell QDs. For $CdS/AgZnSe_{599}$ and $CdS/AgZnSe_{601}$, we observed significant changes in the peak position when compared to the CdS core. Specifically, the peak position of $CdS/AgZnSe_{599}$ exhibited similar frequency to CdS LO frequency but the peak at the CdS overtone region was more blue-shifted in frequency. Conversely, the peak frequencies of $CdS/AgZnSe_{599}$ relative to CdS LO and the overtone region were more red-shifted in comparison to the CdS core. The degree of frequency shift in $CdS/AgZnSe_{599}$ and $CdS/AgZnSe_{601}$ peak position relative to CdS can be understood in terms of the growth morphology and the degree of interfacial defect states in the QDs. Thus, the frequency shift and strain relaxation in the core/alloyed shell interface will differ due to the QDs size and shell thickness. The relatively less-pronounced peaks below 220 cm^{-1} for the core/alloyed shell QDs can be ascribed to a surface optical phonon feature which is inherent in

finite sized crystals and also from the varying degree of alloying at the interface between CdS core and AgZnSe shell **[45,46]**. The variation in the intensity of the modes below 220 cm^{-1} could probably also account for the differences in alloying efficiency of the AgZnSe shell relative to the CdS core.

3.3. Optical properties

The QDs surface is influenced by the nature and chemical reaction of the synthetic constituents (surfactants, capping ligands and solvents) used in fabricating its structure. The atomistic effects of these constituents form the basis for assessing the quality of the QDs surface as it relates to the optical properties, such as the PL stability, spectral features and PL QY. The formation of midgap, deep and shallow states as surface traps provides the basis to which nonradiative electron-hole recombination degrades the QDs fluorescence. The suppression or total elimination of surface trap states in core QDs via coating of a shell layer is useful for light-associated applications and it provides a platform for better understanding of synthetic fabrication strategies required to construct high-quality QD nanocrystals. Our objective is to investigate the influence of a new shell layer (AgZnSe) on the luminescent properties of colloidal CdS QDs. We have utilized the shell alloying process to unravel how the QDs band gap and synthetic fabrication strategy influences the PL properties of CdS/AgZnSe core/alloyed shell QDs. The PL QY was determined according to the equation:

$$\Phi_{\mathrm{F}}^{\mathrm{QD}} = \Phi_{\mathrm{F}}^{\mathrm{Std}} \frac{\mathrm{F}_{QDs} \cdot \mathrm{OD}_{\mathrm{Std}(\lambda \mathrm{exc})} \cdot \mathrm{n}^2{}_{\mathrm{water}}}{\mathrm{F}_{Std.} \mathrm{OD}_{\mathrm{QD}(\lambda \mathrm{exc})} \cdot \mathrm{n}^2_{\mathrm{ethanol}}} \quad (1)$$

Where Φ_F^{Std} is the PL quantum yield of rhodamine 6G standard in ethanol (Φ = 0.95); F_{Std} and F_{QDs} are the integrated sum of the fluorescence intensity of the standard and QDs; $OD_{QD_{(\lambda exc)}}$ and $OD_{Std_{(\lambda exc)}}$ are the optical densities of the QDs and standard while $n^2_{ethanol}$ and $n^2{}_{water}$ are the refractive indices of ethanol and water used to prepare the standard and QDs respectively.

Fig. 6A and B shows the evolution of the PL emission and absorption spectra of three different-sized CdS core QDs and Table 1 summarizes the corresponding photophysical properties as they relate to the absorption wavelength maximum, full width at half maximum (FWHM), band gap and PL QY. We harvested three-sized CdS core QDs with the sole aim of assessing their optical properties in comparison to the different-sized CdS/AgZnSe core/alloyed shell QDs. A small red shift in PL emission was observed for the harvested different-sized CdS core QDs with the absorption wavelength maximum and FWHM increasing in relation to the core size. The striking feature is the low PL QY which was increasingly tuned from 4 to 16% and also dependent on each core size. We observed that CdS_{471} produced the highest PL QY of 16% while the lowest PL QY value of 4% was exhibited by CdS_{478}. Based on the relatively low PL QY, CdS core QDs suffers significantly from interfacial surface defects and residual strain in which the degree of defect states depends on the core size.

To effectively understand the effect of ternary AgZnSe shell alloying on the PL properties of CdS QDs, we employed two synthetic fabrication strategies. The most obvious and direct evidence of shell alloying comes from the PL emission and absorption spectra shown in Fig. 6C. The evolution of the PL emission of CdS/AgZnSe QDs synthesized via method 1 was tuned from 588 to 601 nm while the absorption spectra (Fig. 6D) was tuned from 464 nm to 477 nm. AgZnSe shell precursors used in method 1 synthesis of CdS/AgZnSe QDs was added into the growth solution after harvesting fraction of CdS_{481} core QDs. The striking feature is the blue-shifted absorption

wavelength and corresponding red shift in PL emission of CdS/AgZnSe$_{588}$ relative to CdS$_{481}$ QDs. The shift reveals that the shell alloying strategy, induced bad gap modulation of the QDs in the visible region of the electromagnetic spectrum. For CdS/AgZnSe QDs synthesized via method 2, the PL emission spectra was tuned from 591 to 612 nm (Fig. 7A) while the absorption spectra were tuned from 449 to 481 (Fig. 7B). Despite the PL emission being more red-shifted relative to the CdS core, the absorption spectrum of CdS/AgZnSe$_{591}$ was significantly blue-shifted. From Table 1, the efficiency of band gap modulation of CdS/AgZnSe QDs was observed to vary narrowly from 2.07–2.11 eV for method 1 synthesis and from 2.03–2.10 eV for method 2 synthesis of the QDs.

To determine if the band gap modulation of CdS/AgZnSe QDs originated from the intrinsic optical properties of the core/alloyed nanostructures, a deeper assessment of the PL QY values (Table 1) was performed. The most striking observation is the variation in the PL QY of CdS/AgZnSe QDs synthesized via method 1 and 2 and the remarkable increase in comparison to the values obtained for CdS core. Via method 1 synthesis, the PL QY of CdS/AgZnSe QDs was tuned from 48 to 51% but via method 2 synthesis the PL QY was tuned from 35 to 73%. It is noteworthy that shell alloying of CdS QDs suppressed interfacial defect states in the core/alloyed shell nanocrystals due to the remarkable increase in the PL QY. However, it is important to emphasize that the defect state suppression efficiency varied amongst the QDs size and was dependent on the quality of the fabrication method.

Examining closely how the shell alloying process influenced the optical properties of the QDs, we have probed the correlation between the band gap modulation and the PL QY. It is a well-established phenomenon that a semiconductor band gap can be reduced by residual strain, thus leading to deformed potential **[47,48].** Therefore, the low PL QY reveals that CdS core QDs suffer

from residual strain due to surface traps embedded within the nanocrystals. The narrow band gap (2.07–2.11 eV) exhibited by the different-sized CdS/AgZnSe QDs (synthesized via method 1), correlated precisely to the small difference in PL QY (48-51%). This suggests that suppression of surface defect states in CdS QDs was with a very small margin across the core/alloyed shell QDs size. However, a wider margin in defect state suppression was observed for CdS/AgZnSe QDs synthesized via method 2, due to the wider difference in PL QY from 35% to 73%. Two important features are the maximum PL QY of 73% and the precise correlation in the margin of difference between the band gap and the PL QY. It is also noteworthy that the high PL QY implies much of the surface defects were suppressed by the shell alloying process while the variation in PL QY correlated precisely to the efficiency of surface defect suppression.

4. Conclusions

The passivation of CdS QDs with a new ternary alloyed AgZnSe shell layer was obtained via the organometallic synthetic route. The band gap of CdS/AgZnSe core/alloyed shell QDs was tuned across the visible region with the nanocrystals exhibiting varying PL QYs. We observed a precise correlation in the margin of difference between the band gap of the QDs and the PL QY. The effect of shell alloying was observed in the QDs growth morphology in which the QDs growth transitioned from a homogeneous state to a heterogeneous state. Transition in the phase structure of the QDs from a zinc blende diffraction pattern to a wurtzite diffraction pattern was also observed. Generally, we have established that AgZnSe shell passivation on luminescent CdS QDs suppressed interfacial defect states in the CdS core QDs with the degree of suppression dependent on the size of the QDs derived from the finely-tuned synthetic fabrication strategy.

Acknowledgement

Financial support from the Water Research Council (WRC) project K5/2752, South Africa and the University of Pretoria is gratefully acknowledged.

Reference

[1] T.V. Duncan, M.A. Mendez Polanco, Y. Kim and S.-J. Park, Improving the quantum yields of semiconductor quantum dots through photoenhancement assisted by reducing agents, J. Phys. Chem. C, 11 (2009) 7561–7566.

[2] A. Hassinen, I. Moreels, K. De Nolf, P.F. Smet, J.C. Martins and Z. Hens, Short-chain alcohols strip X-type ligands and quench the luminescence of PbSe and CdSe Quantum dots, acetonitrile does not, J. Am. Chem. Soc. 134 (2012) 20705–20712.

[3] M. Nasilowski, P. Spinicelli, G. Patriarche, B. Dubertret, Gradient CdSe/CdS quantum dots with room temperature biexciton unity quantum yield, Nano Lett. 15 (2015) 3953−3958.

[4] P. Reiss, M. Protière, L. Li, Core/shell semiconductor nanocrystals, Small 5 (2009) 154−168.

[5] D.V. Talapin, J.-S. Lee, M.V. Kovalenko, E.V. Shevchenko, Prospects of colloidal nanocrystals for electronic and optoelectronic applications. Chem. Rev. 110 (2010) 389−458.

[6] O. Chen, J. Zhao, V.P. Chauhan, J. Cui, C. Wong, D.K. Harris, H. Wei, H.-S. Han, D. Fukumura, R.K. Jain, M.G. Bawendi, Compact high-quality CdSe−CdS core−shell nanocrystals with narrow emission linewidths and suppressed blinking. Nat. Mater. 12 (2013) 445−451.

[7] C. Giansante, I. Infante, Surface traps in colloidal quantum dots: a combined experimental and theoretical perspective, J. Phys. Chem. Lett. 8 (2017) 5209−5215.

[8] M. Nirmal, B.O. Dabbousi, M.G. Bawendi, J.J. Macklin, J.K. Trautman, T.D. Harris, L.E. Brus, Fluorescence intermittency in single cadmium selenide nanocrystals, Nature 383 (1996) 802−804.

[9] A. Efros, M. Rosen, Random telegraph signal in the photoluminescence intensity of a single quantum dot, Phys. Rev. Lett. 78 (1997) 1110−1113.

[10] Y. Altintas, M.Y. Talpur, M. Ünlü, E. Mutlugün, Highly efficient cd-free alloyed core/shell quantum dots with optimized precursor concentrations, J. Phys. Chem. C 120 (2016) 7885−7892.

[11] J. Bang, J. Park, J.H. Lee, N. Won, J. Nam, J. Lim, B.Y. Chang, H.J. Lee, B. Vhon, J. Shin, J.B. Park, .H. Choi, K. Cho, S.M. Park, T. Joo, S. Kim, ZnTe/ZnSe (core/shell) type-ii quantum dots: their optical and photovoltaic properties, Chem. Mater. 22 (2010) 233–240.

[12] M.D. Tessier, D. Dupont, K. De Nolf, J. De Roo, Z. Hens, Economic and Size-tunable synthesis of InP/ZnE (E = S, Se) colloidal quantum dots, Chem. Mater. 27 (2015) 4893−4898.

[13] W. Jiang, A. Singhal, J. Zheng, C. Wang, W.C.W. Chan, Optimizing the synthesis of red- to near-ir-emitting CdS-capped $CdTe_xSe_{1-x}$ alloyed quantum dots for biomedical imaging, Chem. Mater. 18 (2006) 4845-4854.

[14] P. Tyagi, P. Kambhampati, Independent control of electron and hole localization in core/barrier/shell nanostructures, J. Phys. Chem. C, 116 (2012) 8154–8160.

[15] M. Nasilowski, P. Spinicelli, G. Patriarche, B. Dubertret, Gradient CdSe/CdS quantum dots with room temperature biexciton unity quantum yield. Nano Lett. 15 (2015) 3953−3958.

[16] M. Wang, M. Zhang, J. Qian, F. Zhao, L. Shen, G.D. Scholes, M.A. Winnik, Enhancing the photoluminescence of polymer-stabilized CdSe/CdS/ZnS core/shell/shell and CdSe/ZnS

core/shell quantum dots in water through a chemical-activation approach, Langmuir 25 (2009) 11732–11740.

[17] W. Liu, H. Soo Choi, J.P. Zimmer, E. Tanaka, J.V. Frangioni, M. Bawendi, Compact cysteine-coated CdSe(ZnCdS) quantum dots for in vivo applications, J. Am. Chem. Soc. 129 (2007) 14530-14531.

[18] K. Yu, S. Singh, N. Patrito, V. Chu, Effect of reaction media on the growth and photoluminescence of colloidal CdSe nanocrystals, Langmuir 20 (2004) 11161-11168.

[19] R.E. Bailey, S. Nie, Alloyed semiconductor quantum dots: tuning the optical properties without changing the particle size, J. Am. Chem. Soc. 125 (2003) 7100-7106.

[20] J. Quyang, C.I. Ratcliffe, D. Kingston, B. Wilkinson, J. Kuijper, X. Wu, J.A. Ripmeester, K. Yu, Gradiently alloyed $Zn_xCd_{1-x}S$ colloidal photoluminescent quantum dots synthesized via a noninjection one-pot approach, J. Phys. Chem. C 112 (2008) 4908-4919.

[21] R. Gui, A. Wan, H. Jin, H. Li, C. Zhou, Acetyl acetonate-stabilized $Mn2^{+}$:CdS quantum dots: Aqueous synthesis and reversible fluorescence tuned by redox reaction, Mater. Lett. 98 (2013) 190-193.

[22] R. Gui, X. An, H. Su, W. Shen, Z. Chen, X. Wang, A near-infrared-emitting CdTe/CdS core/shell quantum dots-based OFF–ON fluorescence sensor for highly selective and sensitive detection of $Cd2^{+}$, Talanta 94 (2012) 257-262.

[23] R. Gui, X. An, Layer-by-layer aqueous synthesis, characterization and fluorescence properties of type-II CdTe/CdS core/shell quantum dots with near-infrared emission. RSC Adv. 3 (2013) 20959-20969.

[24] M.V. Rama Krishna, R.A. Friesner, Quantum confinement effects in semiconductor clusters, J. Chem. Phys. 95 (1991) 8309-8322.

[25] I. Hernandez-Calderon, II-VI Semiconductor Materials and Their Applications, (Ed. Tamargo, M. C.), P136-138, Vol. 12 in Optoelectronic Properties of Semiconductors and Superlattices; Manasreh, M. O., Ed.; Taylor & Francis Inc.: New York, 2002.

[26] A. I. Ekimov, I. A. Kudryavtsev, M. G. Ivanov, A.L. Efros, Spectra and decay kinetics of radiative recombination in CdS microcrystals, J. Lumin. 46 (1990) 83-95.

[27] K. Gong, D.F. Kelley, Lattice strain limit for uniform shell deposition in zincblende CdSe/CdS quantum dots, J. Phys. Chem. Lett. 6 (2015) 1559−1562.

[28] C.-C. Hung, S.-J. Ho, C.-W. Yeh, G.-H. Chen, J.-H. Huang, H.-S. Chen, Highly luminescent dual-color-emitting alloyed [$Zn_xCd_{1-x}Se_yS_{1-y}$] quantum dots: investigation of bimodal growth and application to lighting, J. Phys. Chem. C 121 (2017) 28373−28384.

[29] L.A. Swafford, L.A. Weigand, M.J. Bowers, J.R. McBride, J.L. Rapaport, T.L. Watt, S.K. Dixit, L.C. Feldman, S.J. Rosenthal, Homogeneously alloyed CdS_xSe_{1-x} nanocrystals: synthesis, characterization, and composition/size-dependent band gap, J. Am. Chem. Soc. 128 (2006) 12299.

[30] Z. Pan, K. Zhao, J. Wang, H. Zhang, YY. Feng, X. Zhong, Near infrared absorption of $CdSe_xTe_{1-x}$ alloyed quantum dot sensitized solar cells with more than 6% efficiency and high stability, ACS Nano 7 (2013) 5215–5222.

[31] A. Kigel, M. Brumer, A. Sashchiuk, L. Amirav, E. Lifshitz, $PbSe/PbSe_xS_{1-x}$ core-alloyed shell nanocrystals, Mater. Sci. Eng., C 25 (2005) 604-608.

[32] H. Jin, R. Gui, Z. Wang, J. Xia, M. Yang, F. Zhang, S. Bi, Facile fabrication of water-dispersible $AgInS_2$ quantum dots and mesoporous $AgInS_2$ nanospheres with visible photoluminescence, RSC Adv. 5 (2015) 68287-68292.

[33] P. Yang, M. Ando, N. Murase, Highly luminescent CdSe/$Cd_xZn_{1-x}S$ quantum dots coated with thickness-controlled SiO_2 shell through silanization, Langmuir 27 (2011) 9535–9540.

[34] K. Boldt, N. Kirkwood, G.A. Beane, P. Mulvaney, Synthesis of highly luminescent and photo-stable, graded shell CdSe/$Cd_xZn_{1-x}S$ nanoparticles by in situ alloying, Chem. Mater. 25 (2013) 4731−4738.

[35] S.M. Fairclough, E.J. Tyrrell, D.M. Graham, P.J.B. Lunt, S.J.O. Hardman, A. Pietzsch, F. Hennies, J. Moghal, W.R. Flavell, A.A.R. Watt, J.M.J. Smith, Growth and characterization of strained and alloyed Type-II ZnTe/ZnSe core–shell nanocrystals, Phys. Chem. C 16 (2012) 26898−26907.

[36] W.K. Bae, L.A. Padilha, Y.-S. Park, H. McDaniel, I. Robel, J.M. Pietryga, V.I. Klimov, Controlled alloying of the core-shell interface in CdSe/CdS quantum dots for suppression of Auger recombination, ACS Nano 7 (2013) 3411−3419.

[37] O. Adegoke, K. Takemura, E.Y. Park, Plasmonic oleylamine-capped gold and silver nanoparticle-assisted synthesis of luminescent alloyed CdZnSeS quantum dots, ACS Omega 3 (2018) 135-1366.

[38] J. Quyang, C.I. Ratcliffe, D. Kingston, B. Wilkinson, J. Kuijper, X. Wu, J.A. Ripmeester, K. Yu, Gradiently alloyed $Zn_xCd_{1-x}S$ colloidal photoluminescent quantum dots synthesized via a noninjection one-pot approach, J. Phys. Chem. C 112 (2008) 4908-4919.

[39] B.O. Dabbousi, . Rodriguez-Viejo, F.V. Mikulec, J.R. Heine, H. Mattoussi, R. Ober, K.F. Jensen, M.G. Bawendi, (CdSe)ZnS core-shell quantum dots: synthesis and characterization of a size series of highly luminescent nanocrystallites, J. Phys. Chem. B 101 (1997) 9463-9475.

[40] D.V. Talapin, I. Mekis, S. Götzinger, A. Kornowski, O. Benson, H. Weller, CdSe/CdS/ZnS and CdSe/ZnSe/ZnS core-shell-shell nanocrystals, J. Phys. Chem. B 108 (2004) 18826-18831.

[41] P.T.K. Chin, C. de Mello Donega, S.S. van Bavel, S.C.J. Meskers, N.AJ.M. Sommerdijk, R.A.J. Janssen, Highly luminescent CdTe/CdSe colloidal heteronanocrystals with temperature-dependent emission color, J. Am. Chem. Soc. 129 (2007) 14880-14886.

[42] N.T.K. Thanh, N. Maclean, S. Mahiddine, Mechanisms of nucleation and growth of nanoparticles in solution, Chem. Rev. 114 (2014) 7610−7630.

[43] F.; Garcia-Santamaría, S. Brovelli, R. Viswanatha, J.A. Hollingsworth, H. Htoon, S.A. Crooker, V.I. Klimov, Breakdown of volume scaling in Auger recombination in CdSe/CdS heteronanocrystals: the role of the core-shell interface, Nano Lett. 11 (2011) 687−693.

[44] G.E. Cragg, A.L. Efros, Suppression of auger processes in confined structures, Nano Lett. 10 (2009) 313−317.

[45] F. Comas, N. Studart, G.E. Marques, Optical phonons in semiconductor quantum rods, Solid State Commun. 130 (2004) 477−480.

[46] H. Lange, M. Artemyev, U. Woggon, C. Thomsen, Geometry dependence of the phonon modes in CdSe nanorods, Nanotechnology 20 (2009) 045705.

[47] J. Kim, M.V. Fischetti, Electronic band structure calculations for biaxially strained Si, Ge, and III-V Semiconductors. J. Appl. Phys. 108 (2010) 013710.

[48] J. Kim, M.V. Fischetti, S. Aboud, Structural, electronic, and transport properties of silicane nanoribbons. Phys. Rev. B 86 (2012) 205323.

Table 1. Summary of the photophysical properties of the different-sized CdS core and CdS/AgZnSe QDs.

QDs-λ_{Emi} (nm)	λ_{Abs} (nm)	FWHM (nm)	Band gap (eV)	PL QY (%)
CdS_{471}	458	20	2.64	16
CdS_{478}	471	26	2.60	4
CdS_{481}	476	33	2.58	8
[a]$CdS/AgZnSe_{588}$	464	41	2.11	48
[b]$CdS/AgZnSe_{591}$	449	34	2.10	73
[a]$CdS/AgZnSe_{593}$	468	42	~2.10	50
[a]$CdS/AgZnSe_{599}$	473	40	2.07	49
[a]$CdS/AgZnSe_{601}$	477	45	~2.07	51
[b]$CdS/AgZnSe_{602}$	473	39	2.06	35
[b]$CdS/AgZnSe_{612}$	481	40	2.03	42

[a] Method 1 synthesis

[b] Method 2 synthesis

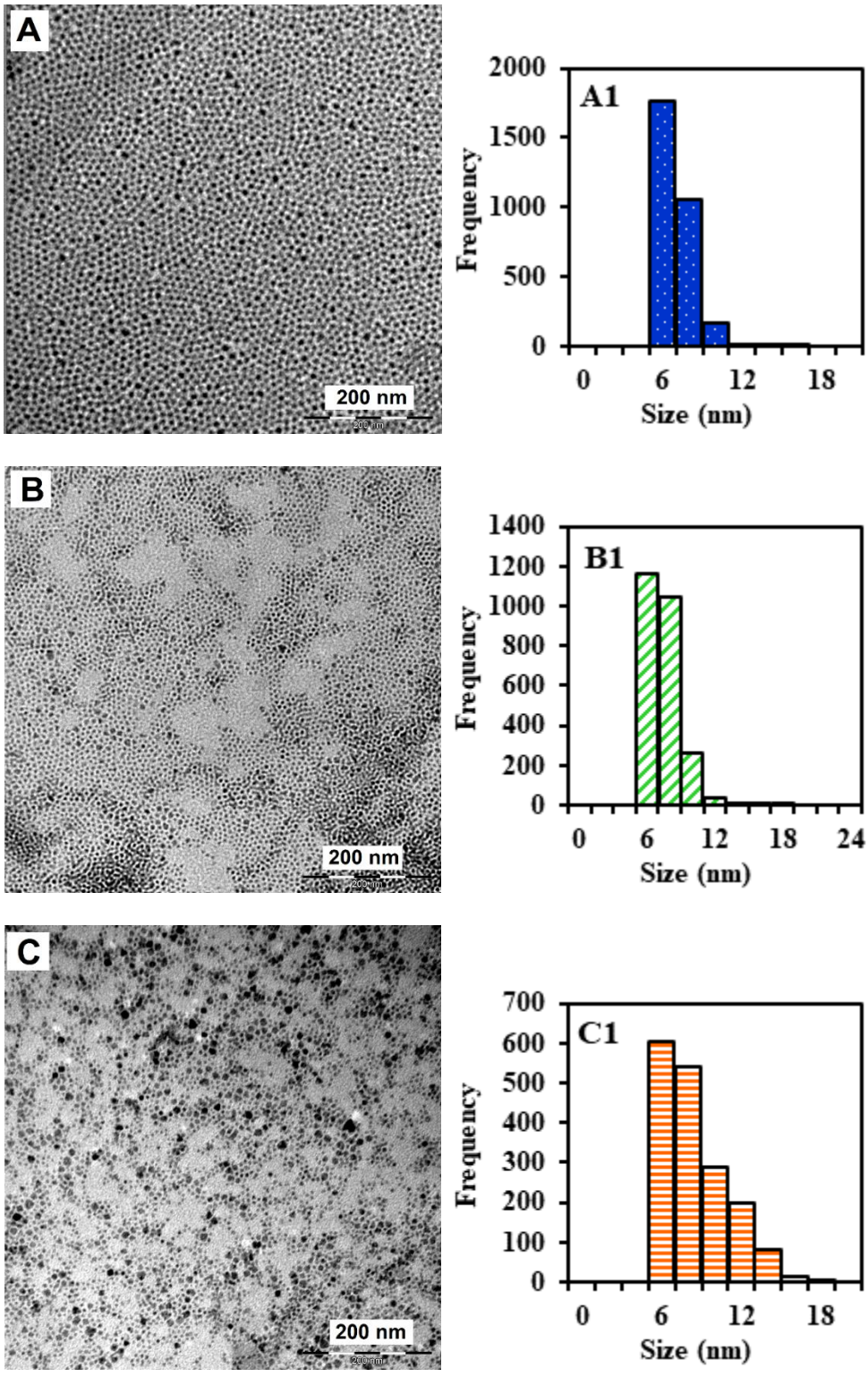

Fig. 1. TEM images (A, B and C) and average particle size distribution (A1, B1 and C1) of CdS core QDs.

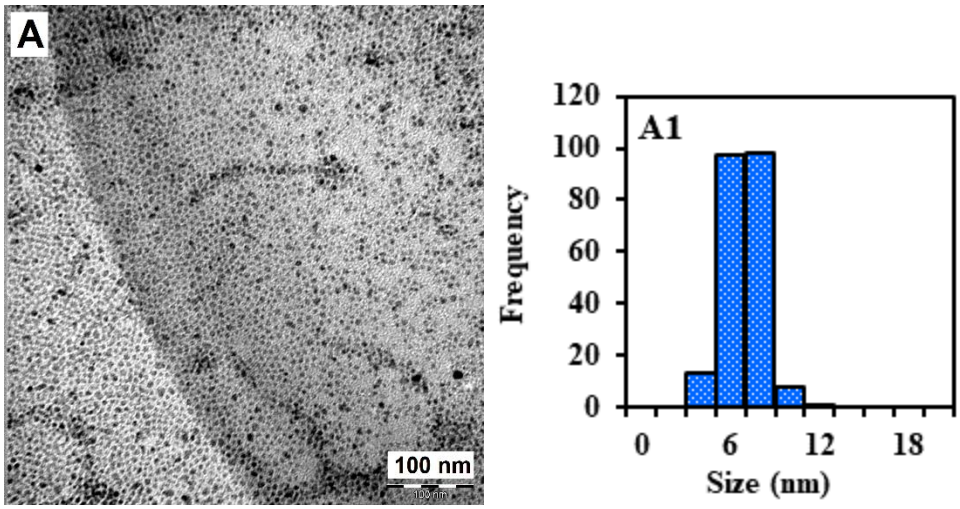

537

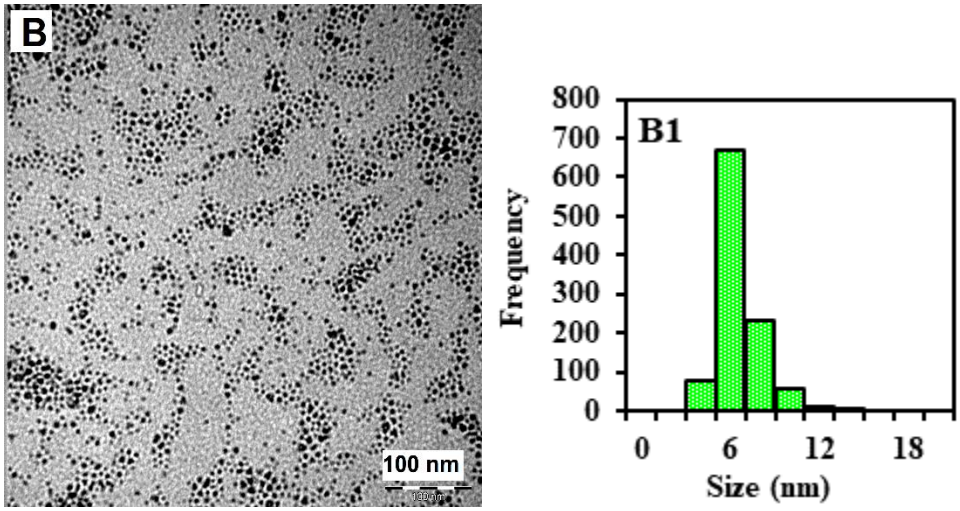

538

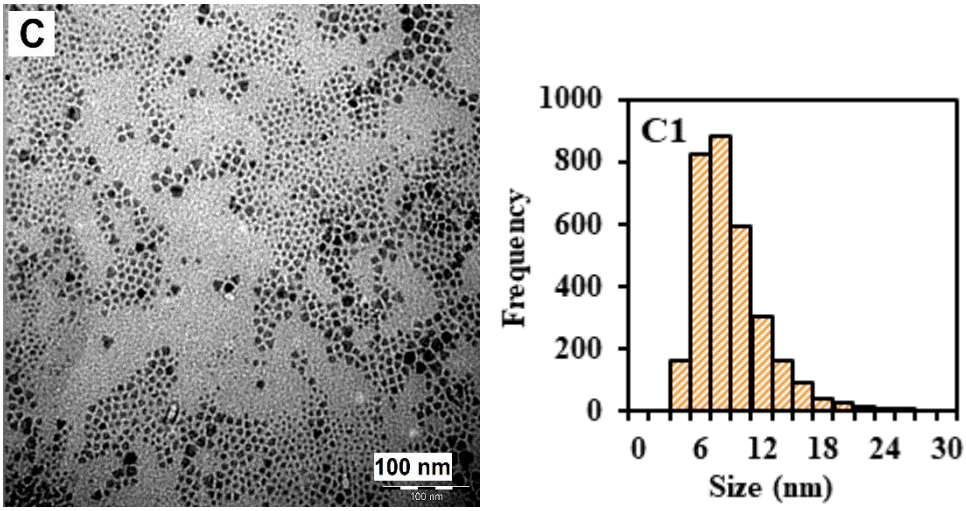

539

540

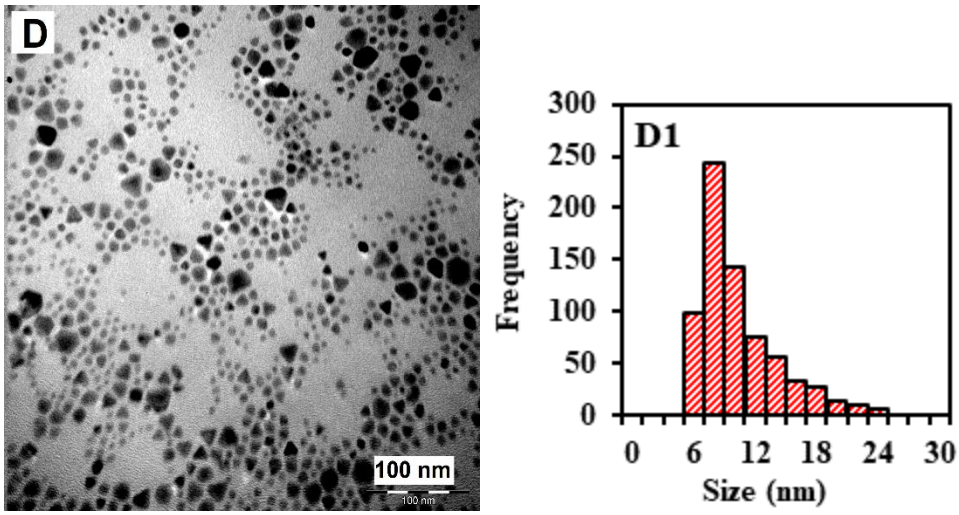

Fig. 2. TEM images (A, B, C and D) and average particle size distribution (A1, B1, C1 and D1) of CdS/AgZnSe core/alloyed shell QDs synthesized via method 1.

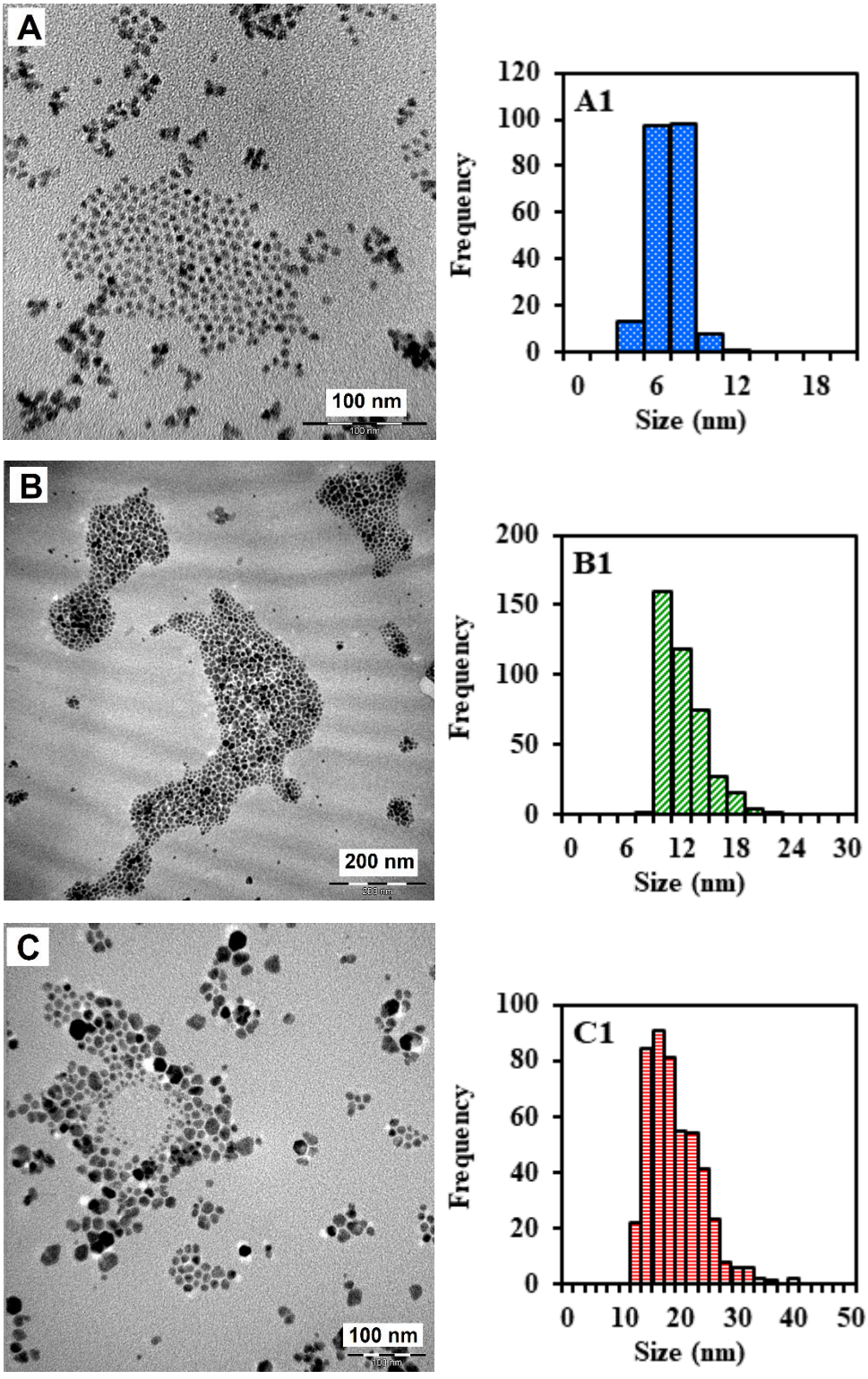

Fig. 3. TEM images (A, B and C) and average particle size distribution (A1, B1 and C1) of CdS/AgZnSe core/alloyed shell QDs synthesized via method 2.

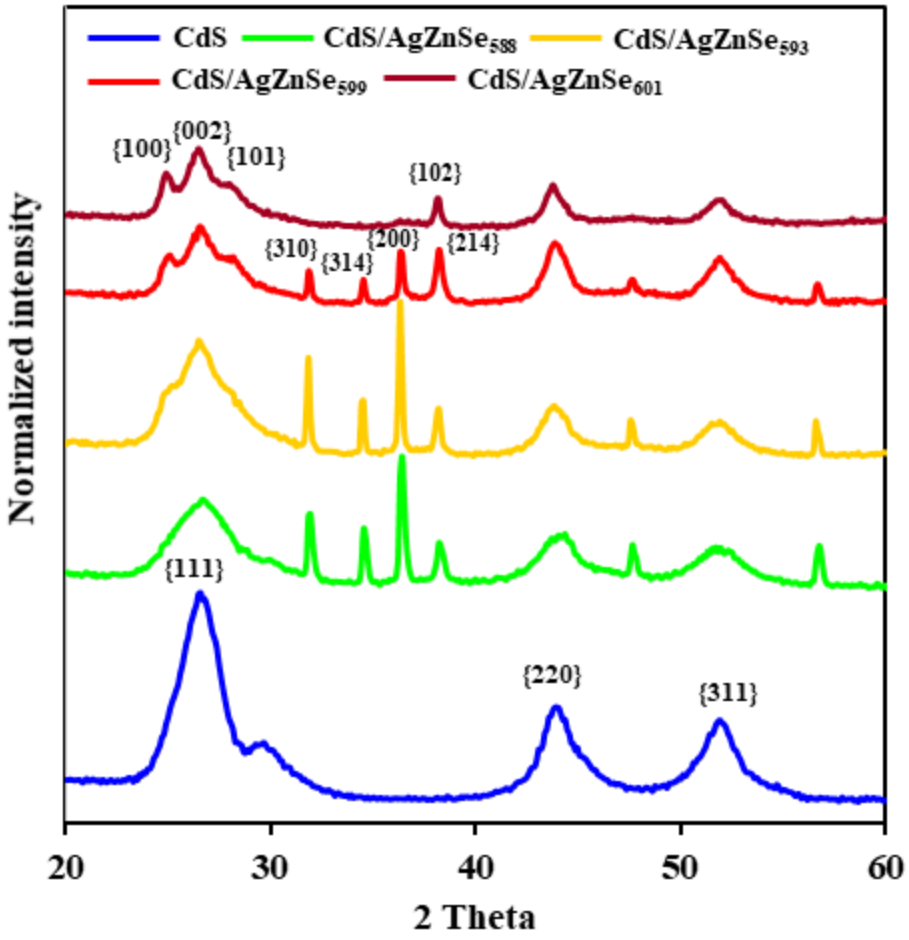

Fig. 4. PXRD plots of CdS, CdS/AgZnSe$_{588}$, CdS/AgZnSe$_{593}$, CdS/AgZnSe$_{599}$ and CdS/AgZnS$_{601}$ QDs.

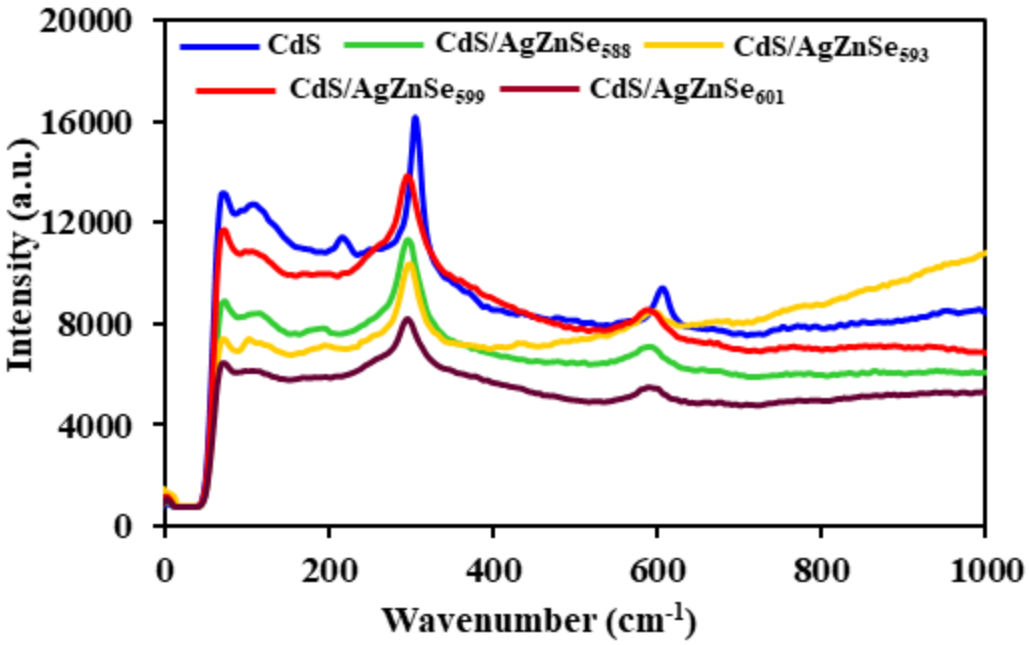

572

573 **Fig. 5.** Raman spectra of CdS, CdS/AgZnSe$_{588}$, CdS/AgZnSe$_{593}$, CdS/AgZnSe$_{599}$ and

574 CdSe/AgZnS$_{601}$ QDs.

575

576

577

578

579

580

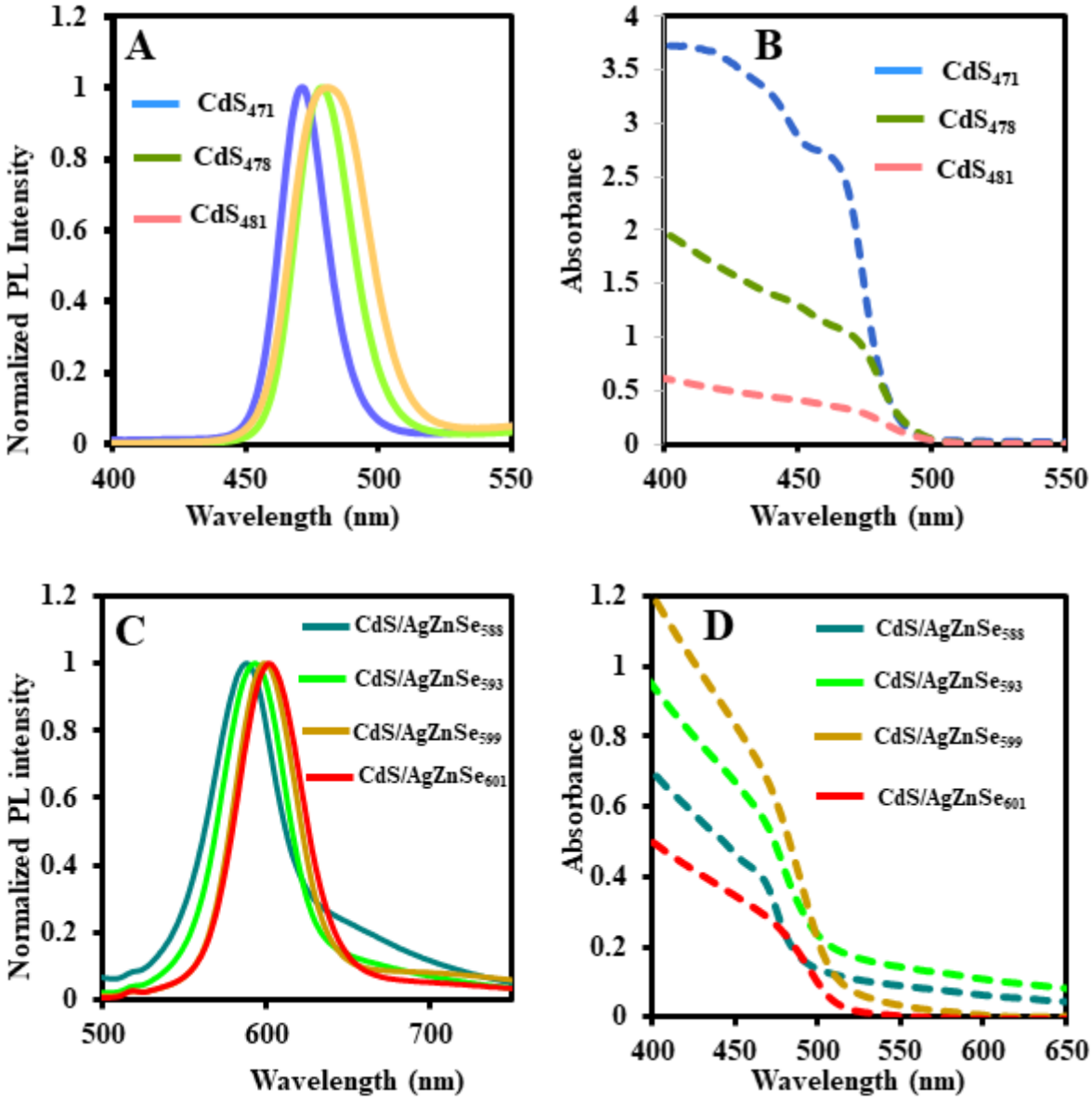

Fig. 6. PL and UV/vis absorption spectra of the different sized CdS (A and B) and CdS/AgZnSe core/alloyed shell QDs (C and D) synthesized via method 1.

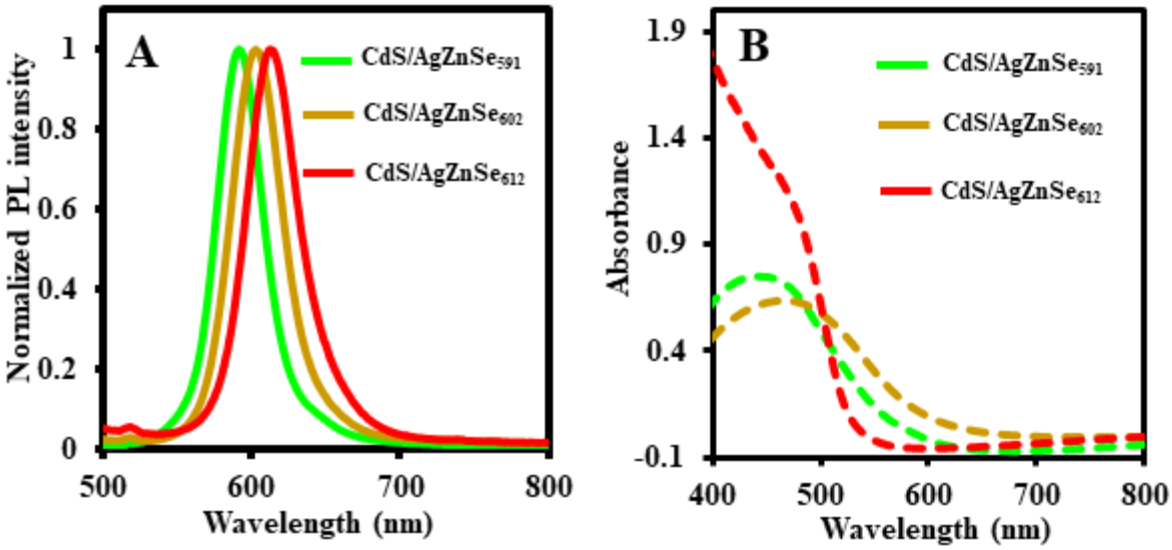

Fig. 7. PL (A) and UV/vis absorption (B) spectra of the different sized and CdS/AgZnSe core/alloyed shell QDs synthesized via method 2.